Review

International Journal of Modern Physics B
Vol. 19, No. 26 (2005) 3897–3921

World Scientific
www.worldscientific.com

TRANSLATIONAL ENTANGLEMENT AND TELEPORTATION OF MATTER WAVEPACKETS BY COLLISIONS AND HALF-COLLISIONS

L. FISCH, A. TAL and G. KURIZKI

Dept. of Chemical Physics, The Weizmann Institute of Science, Rehovot 76100, Israel

Received 9 September 2005

To date, the translationally-entangled state originally proposed by Einstein, Podolsky and Rosen (EPR) in 1935 has not been experimentally realized for massive particles. Opatrný and Kurizki [*Phys. Rev. Lett.* **86**, 3180 (2000)] have suggested the creation of a position- and momentum-correlated, i.e., translationally-entangled, pair of particles approximating the EPR state by dissociation of cold diatomic molecules, and further manipulation of the EPR pair effecting matter-wave teleportation. Here we aim at setting the principles of and quantifying translational entanglement by collisions and half-collisions. In collisions, the resonance width s and the initial phase-space distributions are shown to determine the degree of post-collisional momentum entanglement. Half-collisions (dissociation) are shown to yield different types of approximate EPR states. We analyse a feasible realization of translational EPR entanglement and teleportation via cold-molecule Raman dissociation and subsequent collisions, resolving both practical and conceptual difficulties it has faced so far: How to avoid entanglement loss due to the wavepacket spreading of the dissociation fragments? How to measure both position and momentum correlations of the dissociation fragments with sufficient accuracy to verify their EPR correlations? How to reliably perform two-particle (Bell) position and momentum measurements on one of the fragments and the wavepacket to be teleported?

Keywords: Entanglement; quantum information; continuous variables; quantum teleportation; molecular dynamics; cold-atom collisions.

PACS numbers: 03.67.Hk, 03.65.Ud, 39.20.+q

1. Introduction

Einstein, Podolsky and Rosen (EPR) suggested the EPR state of two particles with well-defined momentum-sum and position-difference[1] in order to illustrate their dissatisfaction with what they interpreted as the lack of completeness of quantum mechanics. Schröedinger later identified the "paradoxical" features of such a state with two-particle entanglement involving continuous variables.[2] Despite the fact that entanglement and EPR-like correlations have become key notions in contemporary physics, the original EPR scenario[1] has been studied only to a limited

extent, much less than the discrete-variable spin-1/2 entanglement. In studies of continuous-variable EPR entanglement, the accent has been on the electromagnetic field analog of position-momentum uncertainty[3−5] and very recently on coordinate-momentum entanglement of two photons.[6] Mathematically, continuous-variable entanglement has been analyzed using a finite-dimensional basis for systems of *bound* particles,[4] or an infinite, but countable, harmonic-oscillator basis, for field quadratures.[5] The first concrete proposal for measuring position-momentum entanglement of massive unbound particles was made by Opatrný and Kurizki[7] based on molecular-dimer dissociation. They also suggested that a subsequent collision of one of the EPR-entangled dissociation fragments with a wavepacket, followed by Bell-like measurements of their *joint* variables, can be used to teleport the wavepacket.

Here we set a broader aim: understanding and quantifying the entanglement of the translational degrees of freedom of the particles, by studying a ubiquitous class of processes, namely, binary collisions of *unbound particles* based on the recent analysis of Tal and Kurizki[8] and comparing them to half-collisions (bound-state dissociation). We shall address both practical and conceptual difficulties these processes may face:

(1) How to quantify translational entanglement resulting from collisions or half-collisions (dissociation)?
(2) How to avoid entanglement loss due to the wavepacket spreading of the collision or half-collision products?
(3) How to measure position and momentum correlations of the dissociation fragments or collision partners with sufficient accuracy to verify their EPR entanglement?
(4) How to reliably perform two-particle (Bell) position and momentum measurements, jointly on one of the fragments and the wavepacket to be teleported?

The considerations outlined here are common to molecular dissociation,[7,9] dipole-dipole correlations in optical lattices,[10,11] photoionization[12] and cold-atom collisions.[13,14]

EPR states and measures are analysed in Sec. 2. EPR entanglement via collisions is analysed in Sec. 3. The 2-particle wavefunction obtained by half-collisions, with an accent on Raman dissociation, is analyzed and shown to have the EPR characteristics in Sec. 4. This process can occur in an atomic waveguide,[20] which favors 1D translational EPR correlations (Sec. 5.2). We show how to preserve the maximal s value of the post-dissociative freely-spreading wavepacket (Secs. 5.3 and 5.4) by trapping (storing) the 2-atom state in receding potential wells. Verification of translational EPR correlations by measurement of the trapped (stored) atoms, including far-field "ghost diffraction", are proposed in Sec. 6. A possible teleportation protocol using translational EPR correlations is put forward in Sec. 7. Section 8 summarizes our findings. Appendix A derives the 1D post-collision density operator, Appendix B summarizes the relations (rapport) between 2-particle wavepackets prepared via collisions and half collisions. Appendix C evaluates these wavepackets for one- and two- photon (Raman) dissociation.

2. EPR States and Measures

The two possible EPR states of particles 1, 2 with *ideal* coordinate and momentum entanglement will be denoted by $|EPR_{\mp}\rangle$. They satisfy

$$\begin{aligned} \langle x_1, x_2|EPR_{\mp}\rangle &= \delta(x_1 \mp x_2) \\ \langle p_1, p_2|EPR_{\mp}\rangle &= \delta(p_1 \pm p_2) \end{aligned} \tag{1}$$

where $x_{1(2)}$ and $p_{1(2)}$ are the respective coordinates and momenta. Both these states are unrealistic, in that they are unnormalizable and have infinite energy. They may be seen as limits of the "physical" state

$$\langle x_1, x_2|\Psi\rangle = Ne^{-(\frac{x_{\rm cm}}{2\Delta x_{\rm cm}})^2} e^{-(\frac{x_{\rm rel}}{2\Delta x_{\rm rel}})^2} \tag{2}$$

where N is the normalization, $x_{\rm rel} \equiv x_1 - x_2$ and $x_{\rm cm} \equiv \frac{x_1+x_2}{2}$ are the relative and center-of-mass coordinates. The limit $\Delta x_{\rm rel} \to 0, \Delta x_{\rm cm} \to \infty$ yields the EPR$_-$ state and the limit $\Delta x_{\rm rel} \to \infty, \Delta x_{\rm cm} \to 0$ yields its EPR$_+$ counterpart.

The degree to which state (2) approximates the ideal states (1) can be quantified by several criteria:

(a) Opatrný and Kurizki[7] adopted the "squeezing" parameter s, defined as

$$s(t) = \frac{\hbar}{2\Delta x_1^{(c)}(t)\Delta p_1^{(c)}}\,. \tag{3}$$

$\Delta x_1^{(c)}$ is the variance of the *conditional* distribution

$$P(x_1|x_2 = a) = \frac{|\Psi(x_1, x_2 = a)|^2}{P(x_2 = a)}\,, \tag{4}$$

and $P(x_2 = a) = \int dx_1 |\Psi(x_1, x_2 = a)|^2$. Similarly, $\Delta p_1^{(c)}$ is the conditional momentum uncertainty.

Alternatively, the *largest* of $\Delta x_{\rm rel}/\Delta x_{\rm cm}$, or its inverse (likewise for $\Delta p_{\rm rel}/\Delta p_{\rm cm}$) may define $s(t)$ for the Gaussian wavepackets [Eq. (2)]. In the EPR-$_{\mp}$ limit, e.g., $s(t) = \Delta x_{\rm rel}(t)/\Delta x_{\rm cm}(t)$. When approaching the EPR$_+$ limit, we find $\Delta x_1^{(c)} = \min(2\Delta x_{\rm cm}, \Delta x_{\rm rel})$, while near the EPR$_-$ limit, $\Delta p_1^{(c)} = \min(2\Delta p_{\rm cm}, \Delta p_{\rm rel})$. Thus, the parameter s, which is the inverse of what may be termed the "Einstein uncertainty", is an appropriate measure of the EPR correlation for both EPR states, occurring when $s > 1$. As $|\Psi\rangle$ in Eq. (2) *evolves freely*, the c.m. and relative uncertainties in the r_j $(j = 1, 2)$ coordinates grow as $\Delta r_j(t)^2 = \Delta r_j(0)^2 + \Delta p_j^2 t^2/m^2$, and thus the value of s becomes *smaller* with time.

(b) An alternative entanglement measure is the Schmidt number K, which has been adopted in Ref. 3. The Schmidt analysis of a gaussian state of the form (2) yields the result[3]

$$K \equiv \left(\sum_{n=0}^{\infty} \lambda_n^2\right)^{-1} = \frac{1}{2}\left(\frac{\Delta p_{\rm rel}}{2\Delta p_{\rm cm}} + \frac{2\Delta p_{\rm cm}}{\Delta p_{\rm rel}}\right) \tag{5}$$

where λ_n's are the discretized eigenvalues of the single-particle reduced density matrix. It can be shown that K is a constant of the free motion, and thus a useful entanglement measure. It can be represented as[12]

$$K = \frac{\Delta p_1}{\Delta p_1^{(c)}} \,. \tag{6}$$

(c) One may also measure entanglement by the Von-Neumann (VN) entropy, which, for the *discretized* eigenvalues λ_n of the single-particle reduced density matrix, has the form

$$S \equiv -\sum_{n=0}^{\infty} \lambda_n \, \ln \, \lambda_n \,. \tag{7}$$

The evaluation of S for collisions of unbound particles is highly nontrivial, as shown in Sec. 3. For the gaussian state (2), S becomes[3]

$$S = \log \frac{(\Delta x_{\rm rel} + 2\Delta x_{\rm cm})^2}{8\Delta x_{\rm rel}\Delta x_{\rm cm}} + \left| \frac{\Delta x_{\rm rel} - 2\Delta x_{\rm cm}}{4\Delta x_{\rm rel}\Delta x_{\rm cm}} \right| \log \left| \frac{\Delta x_{\rm rel} + 2\Delta x_{\rm cm}}{\Delta x_{\rm rel} - 2\Delta x_{\rm cm}} \right| . \tag{8}$$

In the limit $\Delta x_{\rm cm} \gg \Delta x_{\rm rel}$, this reduces to $S \simeq \log \Delta x_{\rm cm}(t)/\Delta x_{\rm rel}(t) = \log s(t)$.

While gaussian-like wavepackets in the relative and center-of-mass variables are adequately characterized by $s(t)$, both S and K quantify the entanglement of an *arbitrarily-shaped* (non-gaussian) wavepacket, which is common for unbound-particle collisions (Sec. 3).

A recent experiment[6] has demonstrated that $s \sim 10$ is achievable by combining a near-field measurement of $\Delta x_{\rm rel}$ with a far-field measurement of $\Delta p_{\rm cm}$ for photon pairs generated by parametric down conversion. The more formidable challenge examined here is the preparation and measurement of EPR correlations between matter waves, formed by dissociation or a collision.

3. EPR Entanglement via Two-Particle Collisions

3.1. *General description*

Consider two particles, 1 and 2, coupled by a *finite-range* interaction. Assuming that the interaction does not affect their internal states, the initial two-particle *unbound* state, $|\Psi_i\rangle$, evolves, after the interaction (collision) has ceased, as[15]

$$|\Psi_i\rangle \to |\Psi_f\rangle = (U_1(t) \otimes U_2(t))(I_{\rm CM} \otimes \mathsf{S})|\Psi_i\rangle \,, \tag{9}$$

where U_j is the free-evolution propagator of system $j = 1, 2$, $I_{\rm cm}$ is the identity operator of the center-of-mass (CM) motion of the two systems, and S is the scattering matrix for their relative motion. The post-collision single-particle VN entropy is then obtainable as

$$(S_1)_f = -{\rm tr}_1(\rho_1 \, \log_2 \, \rho_1) \,, \tag{10}$$

$$\rho_1 = {\rm tr}_2((I_{\rm CM} \otimes \mathsf{S})|\Psi_i\rangle\langle\Psi_i|(I_{\rm CM} \otimes \mathsf{S})^\dagger) \,, \tag{11}$$

where we have used the VN entropy's invariance under unitary transformations. The entanglement is seen to be a function solely of the scattering matrix and the initial wave function. Since the diagonalization of the continuous-variable reduced density matrix ρ_1, as required to compute $(S_1)_f$, is generally intractable, simplifications and approximations are imperative.

We shall consider two unbound particles of equal mass, such that their relative momentum is related to their individual momenta by $\mathbf{k}_{\rm rel} = \frac{\mathbf{k}_1 - \mathbf{k}_2}{2}$. For three dimensional (3D) collisions, we shall assume that each momentum state $|\mathbf{k}_i\rangle$ can scatter onto a discrete, orthonormal set of final states with momenta $\{\mathbf{k}_f\}_{j=1}^{M}$. The replacement of continuous variables by discrete values of $\mathbf{k}_f$ and $\mathbf{k}_i$ implies the use of momentum wavepackets centered around these values, whose widths are small enough (see below) for the S-matrix elements $\langle \mathbf{k}_f|\mathsf{S}|\mathbf{k}_i\rangle$ to be constant throughout the wavepacket.

Let us take the initial two-particle state to be an entangled superposition

$$|\Psi_i\rangle = \sum_i c_i |\mathbf{k}_i\rangle \otimes |-\mathbf{k}_i\rangle = \sum_i c_i |\mathbf{K}_{\rm CM} = \mathbf{0}\rangle \otimes |\mathbf{k}_{\rm rel} = \mathbf{k}_i\rangle \,. \tag{12}$$

Following the collision, Eq. (12) evolves, according to the superposition principle, into:

$$|\Psi_f\rangle = \sum_i \sum_{\mathbf{k}_f} c_i \langle \mathbf{k}_f|\mathsf{S}|\mathbf{k}_i\rangle |-\mathbf{k}_f\rangle \otimes |\mathbf{k}_f\rangle \tag{13}$$

the sum running over $\mathbf{k}_{\rm rel} = \mathbf{k}_f$. In the resulting post-collision density matrix $|\Psi_f\rangle\langle\Psi_f|$ of the system, particle 2 can be traced out to yield the single-particle (reduced) post-collision density operator $(\rho_1)_f = \sum_{\mathbf{k}_f} |\sum_i \langle \mathbf{k}_f|\mathsf{S}|\mathbf{k}_i\rangle|^2 |\mathbf{k}_f\rangle\langle\mathbf{k}_f|$.

On the other hand, the initial single-particle entropy in the state (12) is readily seen to be $(S_1)_i = -\sum_i |c_i|^2 \log_2 |c_i|^2$. Hence, to zeroth order in the momentum widths of the initial wavepackets, the change $\triangle S_1^{(0)}$ in the VN entropy of particle 1 as a result of the collision is:

$$\triangle S_1^{(0)} = -\sum_{\mathbf{k}_f} \left| \sum_i c_i \mathsf{S}_{\mathbf{k_f},\mathbf{k_i}} \right|^2 \log_2 \left(\left| \sum_i c_i \mathsf{S}_{\mathbf{k_f},\mathbf{k_i}} \right|^2 \right) + \sum_i |c_i|^2 \log_2 |c_i|^2 \,, \tag{14}$$

where $\mathsf{S}_{\mathbf{k},\mathbf{k}'} \equiv \langle \mathbf{k}|\mathsf{S}|\mathbf{k}'\rangle$. In the case $c_1 = 1$, when Eq. (12) has the unentangled (product) form $|\mathbf{k}_i\rangle \otimes |-\mathbf{k}_i\rangle$, Eq. (14) reduces to:

$$\triangle S_1^{(0)} = -\sum_{\mathbf{k}_f} |\mathsf{S}_{\mathbf{k_f},\mathbf{k_i}}|^2 \log_2 (|\mathsf{S}_{\mathbf{k_f},\mathbf{k_i}}|^2) \,. \tag{15}$$

This result is in complete correspondence with the classical Boltzmann law for entropy change in collisions,[16] if we identify $|\mathsf{S}_{\mathbf{k_f},\mathbf{k_i}}|^2$ with the transition probability from an initial to a final momentum state. By contrast, the interferences of different scattering channels in Eq. (12) for two or more $c_i \neq 0$, render $\triangle S_1$ nonclassical.

3.2. *1D collisions*

To investigate this nonclassical behavior in-depth, we shall henceforth restrict ourselves to 1D collisions of two unbound particles with (equal) mass m. The effect of the S-matrix on single-particle momentum eigenkets is then

$$\mathsf{S}|k\rangle = T(k)|k\rangle + R(k)|-k\rangle\,, \tag{16}$$

where $T(k)$ and $R(k)$ are the transmission and reflection coefficients of the interaction potential $V(x_{\rm rel})$, respectively.

The reduced single-particle post-collision density operator in Eq. (A12) (App. A) consists of four terms: two "cross terms" containing R^*T or RT^*, and two direct terms containing RR^* and TT^*. Let us look at one of the cross terms explicitly (the R^*T term):

$$(\rho_1)^{R^*T} \int dk_1 dk_1' |k_1\rangle\langle k_1'| \left[\int dk R^*\left(\frac{k_1'-k}{2}\right) \times \psi_1^*(k)\psi_2^*(k_1')T\left(\frac{k_1-k}{2}\right)\psi_1(k_1)\psi_2(k)\right]. \tag{17}$$

Taking $|\Psi_i\rangle = |\psi_1\rangle\otimes|\psi_2\rangle$, where the initial wavepackets $|\psi_1\rangle, |\psi_2\rangle$ are *orthogonal*, we can simplify Eq. (11) as follows. Since $\psi_1(k)$ is a particle initially moving to the right, confined to $k>0$, and $\psi_2(k)$ is its left-moving counterpart confined to $k<0$, these have no overlaps and the $\int dk$ integration yields 0. Hence we are left with only the "direct" terms:

$$\rho_1 = \rho_1^T + \rho_1^R\,, \tag{18}$$

$$\rho_1^T = \int dk_1 dk_1' dk |k_1\rangle\langle k_1'| \psi_1(k_1)\psi_1^*(k_1')|\psi_2(k)|^2 \times T\left(\frac{k_1-k}{2}\right) T^*\left(\frac{k_1'-k}{2}\right) \tag{19}$$

$$\rho_1^R = \int dk_1 dk_1' dk |k_1\rangle\langle k_1'| \psi_2(k_1)\psi_2^*(k_1')|\psi_1(k)|^2 \times R\left(\frac{k_1-k}{2}\right) R^*\left(\frac{k_1'-k}{2}\right). \tag{20}$$

Thus, the reduced post-collision (1D) density operator splits naturally into "transmitted" and "reflected" parts, which are orthogonal in the sense that $\rho_1^T\rho_1^R = 0$. As a result, the set of eigenvalues of ρ_1 is given by the union of the sets of eigenvalues of ρ_1^T and ρ_1^R.

In order to evaluate the *near-resonance* collisional entanglement, we perform a series expansion of ρ_1^T and ρ_1^R to second order in the momentum spread of the wavepackets, σ. The momentum spread $\Delta k^2 \equiv \langle k-k_0\rangle^2 \sim \sigma^2$, turning Eq. (14) and the eigenvalues corresponding to Eq. (18) into:

$$\triangle S_1^{(2)} = -\lambda_T^{(2)}\,\log_2\,\lambda_T^{(2)} - \lambda_R^{(2)}\,\log_2\,\lambda_R^{(2)} \tag{21}$$

$$\lambda_T^{(2)} = |T(k_0)|^2 + \frac{\Delta k^2}{4}\frac{d^2}{dk^2}|T(k)|^2_{k=k_0} \tag{22}$$

$$\lambda_R^{(2)} = |R(k_0)|^2 - \frac{\Delta k^2}{4}\frac{d^2}{dk^2}|T(k)|^2_{k=k_0}\,. \tag{23}$$

This analysis, verified by the numerical case study below, shows that initial narrow-width wavepackets are expected to yield double-peaks of the entanglement on both sides of a resonance, where $|T(k)|^2 = |R(k)|^2 = \frac{1}{2}$ and $T(k)$ varies strongly, with a non-zero dip at resonance. In limit $\Delta k \to 0$, the entanglement vanishes when $|T(k)| = 1$ (at resonance) or when $|R(k)| = 1$ (both wavepackets are reflected entirely).

We may estimate $\triangle S_1$ for appreciable 1D momentum widths, $\sigma \gg \Gamma$, i.e., when the initial wavepacket width is much larger than that of the resonance. The post-collision wavefunction can then be written as the sum of transmitted and reflected wavepackets, using Eq. (A10). Each wavepacket is initially confined, in k-space, to a 1D region of dimensions $\Delta k \sim \sigma$. After the collision they are modulated by the transmission and reflection coefficients, the smallest scale of change for both given by Γ. Since the smallest scale of change of a function is the largest scale of change of its Fourier-transform, we can deduce that the emerging wavepackets will be confined in x-space to a box of dimensions $\Delta x_j \sim \frac{1}{\Gamma}$. Hence, we may deduce from Eqs. (19)–(21) that

$$(S_j)_{\max} \sim \log_2\left(\frac{\sigma}{\Gamma}\right)(j = 1, 2)\,. \tag{24}$$

However, *the growth of* $(S_1)_{\max}$ *with momentum width* σ *saturates as* σ *exceeds the distance between resonances* (in momentum space).

3.3. *Numerical case study*

In order to corroborate the above analytical estimates, we perform a numerical case study of 1D colliding gaussian wavepackets obeying Eqs. (21)–(23), taking the

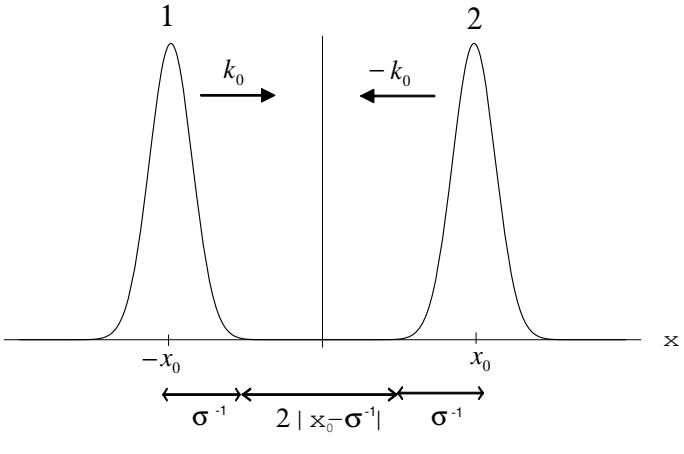

Fig. 1. Schematic illustration of a 1D collision between two wavepackets via a short-range potential, with pre-collision distance $2|x_0 - \sigma|$, momenta $\pm\hbar k_0$ and momentum spread $\hbar\sigma^{-1}$.

interaction potential to be described by a 1D double-delta function of width a,

$$V(x_{\rm rel}) = V[\delta(x_{\rm rel} - a) + \delta(x_{\rm rel} + a)]\,, \tag{25}$$

for which the transmission and reflection coefficients are known to be:

$$T(k) = \frac{4km}{(V\hbar^2 e^{2\imath ak})^2 + (4km + \imath\hbar^2 V)^2} \tag{26}$$

$$R(k) = -\frac{\hbar^2 V(4\imath km(1 + e^{4\imath km}) + (-1 + e^{4\imath km})\hbar^2 V)}{e^{2\imath ak}[e^{4\imath km}\hbar^4 V^2 + (4km + \imath\hbar^2 V)^2]}\,. \tag{27}$$

The initial wavefunctions are taken to be two distant, counter-propagating gaussians, $\psi_{1,2}(k) = \left(\frac{1}{\pi\sigma^2}\right)^{1/4} e^{-\frac{(k\mp k_0)^2}{2\sigma^2} \pm \imath k x_0}$, with $x_0 < 0$, $k_0 > 0$. Note that this implies $k_{\rm rel_0} = \frac{k_{01} - k_{02}}{2} = k_0$. Finding the eigenvalues of ρ_1^T (or ρ_1^R) involves solving an integral equation of the form

$$\int_{-\infty}^{\infty} dk' \rho_1^{T(R)}(k, k')\phi_\lambda(k') = \lambda_T \phi_\lambda(k)\,, \tag{28}$$

where ϕ_λ are the eigenvectors and

$$\rho_1^{T(R)}(k, k') \equiv \langle k|\rho_1^{T(R)}|k'\rangle \tag{29}$$

is the kernel of $\rho_1^{T(R)}$. Examining Eq. (19), we note that $\rho_1^T(k, k')$ becomes negligible for $|k - k_0| \gg \sigma$ and $|k' + k_0| \gg \sigma$. Hence the integral can be approximated by the finite sum,

$$\sum_{k'=-\infty}^{\infty} \Delta k \rho_1^T(k, k')\phi_\lambda(k') = \lambda\phi_\lambda(k)\,. \tag{30}$$

The problem then reduces to finding the eigenvalues of a square matrix with entries $\Delta k \rho_1^{T\,(R)}(k, k')$, where k and k' range from $\pm k_0 - 3 * \sigma$ to $k_0 + 3 * \sigma$ in steps of δk, which must be much smaller than the scale of change of both the potential and the wave packet, so as to approximate the continuous integration faithfully (to within 99.992%). The analytical $\triangle S_1$, given by Eq. (21), is compared in Fig. 2 with the numerical results of the simulation for different σ. The agreement is very good.

For small initial momentum widths such that $\sigma \ll \Gamma$ [i.e., for the last few peaks in Fig. 2(b)], the numerical results confirm the analytical prediction (21), whereby the entropy must have a dip at resonance, $|T|^2 = 1$. On the other hand, $\triangle S_1$ is *maximal* at resonance for $\sigma \sim \Gamma$ or greater. We must control the spacing of resonances, Δk, and their widths, Γ, in order to attain

$$\Delta k \gg \sigma \gg \Gamma\,, \tag{31}$$

which is the optimal range for large ΔS_1. Hence, practically unlimited ΔS_1, indicating an approximate translational EPR state according to Eq. (10), is anticipated for near-resonant collisions, either if the potential has a *single resonance* only (Δk very large), or if the resonance width Γ is very narrow.

The post-collisional entanglement ΔS_1 is found to be *insensitive to fluctuations* in the initial state and is thus *noise resilient*.

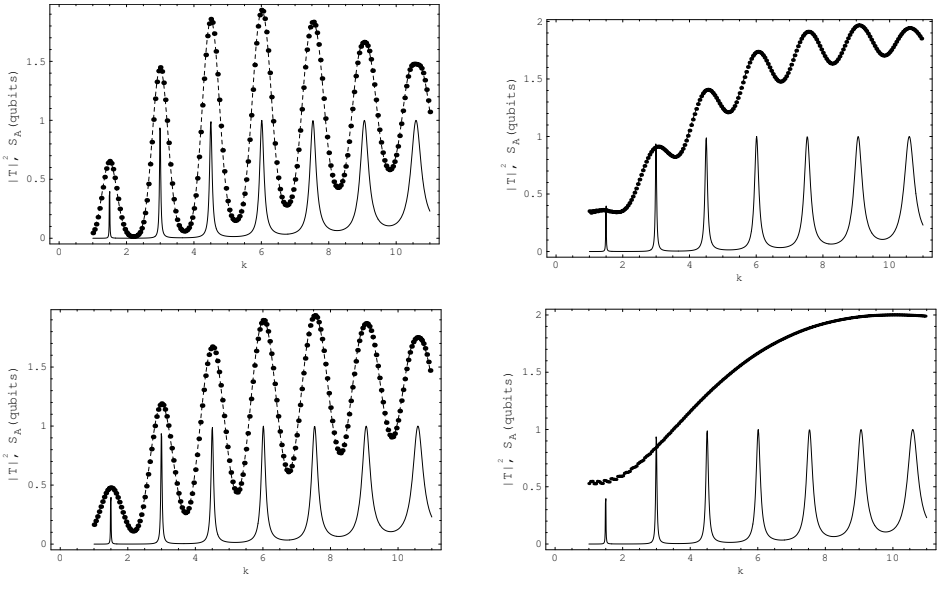

(a)

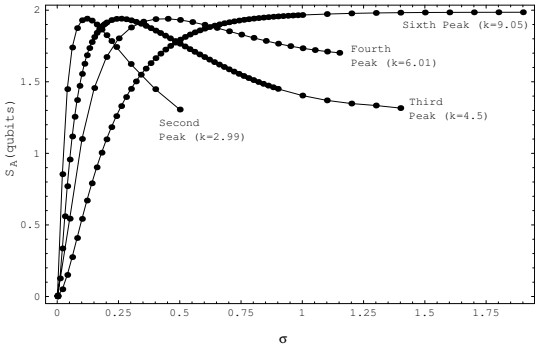

(b)

Fig. 2. (a) Simulation results for the single-particle change in VN entropy, $\triangle S_1$ in 1D collisions for the delta-function potential (25) as a function of the relative momentum. Dotted curves - left, thick curves — right. Thin curves indicate the resonances of the transmission coefficient, the peaks corresponding to $|T|^2 = 1$. Each plot corresponds to another width σ (dashed curves). (b) Variation of the VN entropy as a function of the wavepacket width, σ, for three relative momenta, corresponding to peaks 2, 3 and 5 of the transmission coefficient.

4. Half-Collision (Dissociation) Entanglement

4.1. *General principles*

The two-particle initial state, whether in a collision or a half-collision (dissociation) may be factorized as

$$\langle \mathbf{r}_1, \mathbf{r}_2 | \Psi \rangle = \langle \mathbf{r}_{\rm cm} | \Phi_{\rm cm} \rangle \langle \mathbf{r}_{\rm rel} | \chi_{\rm rel} \rangle \,, \tag{32}$$

where $\mathbf{r}_{\rm cm} = \frac{\mathbf{r}_1+\mathbf{r}_2}{2}$ and $\mathbf{r}_{\rm rel} = \mathbf{r}_1 - \mathbf{r}_2$. This separable form is retained throughout the process.

Quantifying the EPR correlations requires knowledge of the form of $|\Phi_{\rm cm}\rangle$ and $|\chi_{\rm rel}\rangle$, in particular their position and momentum uncertainties along a chosen axis Δx and Δp_x, at asymptotically large distances $r_{\rm rel}$ or times t. An initial wavepacket formed by half-collision or collision, evolves at large $|t|$, in the stationary phase approximation, into

$$\langle \mathbf{r}_{\rm rel}|\chi_{\rm rel}(t)\rangle \to \sum_{l,m}\int dE e^{-i\frac{\hbar k^2 t}{2m}} b_{Elm}(t=0) \times \frac{1}{2ikr}(e^{i(kr-\frac{\pi l}{2})} - e^{-i(kr-\frac{\pi l}{2})})Y_{lm}(\theta,\phi)\,, \tag{33}$$

where $k = \sqrt{2mE_{\rm rel}/\hbar} \equiv k_{\rm rel}$ and b_{Elm} are the initial amplitudes of $|\Psi_{Elm}\rangle$, the eigenstates of the full (scattering) hamiltonian. In what follows we shall consider the resulting x and p_x dispersion for the advantageous process of molecular Raman dissociation. The asymptotic form of $|\chi_{\rm rel}\rangle$ that has emerged from a spherical interaction potential is given by

$$|\chi_{\rm rel}(t\to\infty)\rangle = e^{-iH_0 t/\hbar}\Omega_-^\dagger|\chi_{\rm rel}(0)\rangle = \sum_{l,m}\int dE\langle\Psi_{Elm}|\chi_{\rm rel}(0)\rangle \times e^{i\delta_l(E)}e^{\frac{-iEt}{\hbar}}|\Phi_{Elm}\rangle \tag{34}$$

Here, H_0 is the free Hamiltonian, $\delta_l(E)$ are the scattering phase shifts of the potential waves, $|\Phi_{Elm}\rangle$ and $|\Psi_{Elm}\rangle$ are eigenstates of H_0 and H, the free and scattering Hamiltonian, respectively.

4.2. *Molecular Raman Dissociation*

Raman dissociation uses two c.w. laser beams to force a molecular transition from a bound state to the continuum, via an intermediate bound state on an excited electronic surface,[9] see Fig. 3.

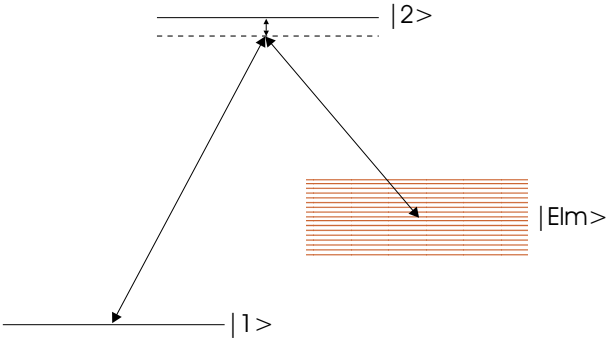

Fig. 3. 3-level model for Raman dissociation.

One obtains (App. C) the spatial form

$$\chi_{\rm rel}(\mathbf{r}_{\rm rel},t)=\sum_{l=0,2}\sqrt{\frac{2l+1}{4\pi}}P_l(\cos\theta)\times\frac{\hbar\Omega_1\Omega^*_{2,E,l}e^{i(k_*r_{\rm rel}-\frac{\pi l}{2}+\delta_l(E)-E_*t/\hbar)}}{2ik_*r_{\rm rel}\Omega_{\rm eff}}$$

$$\times\theta(vt-r_{\rm rel})\,\sin\left(\frac{\Omega_{\rm eff}}{2}\left(t-\frac{r_{\rm rel}}{v}\right)\right)e^{-\frac{\Gamma}{2}(t-\frac{r_{\rm rel}}{v})}\,. \tag{35}$$

This is a first order expansion in the continuum-level detuning. It describes a wavefunction expanding in the direction of growing r, with a sharp edge at $r_{\rm rel}=vt$ and an exponentially falling tail at $r_{\rm rel}<vt$. The radial width of the wavepacket is seen to be v/Γ. Equation (35) exhibits no time-dependent broadening of the wavepacket, which may therefore be treated as its *initial* post-dissociative wavepacket.

The second order expansion yields a much more complicated time-dependent form, displaying dispersion of the wavepacket. An analysis of the typical time- and length-scales[12] shows that

$$t^{(\rm spr)}_{\rm rel}=\mu v^2/\Gamma^2\hbar \tag{36}$$

is the spreading time of the relative-motion wavepacket, which is centered at $r_{\rm rel}\approx vt$. Thus $t/t^{(\rm spr)}_{\rm rel}\approx\frac{\hbar r_{\rm rel}\Gamma^2}{v^3\mu}$ serves as a dimensionless time parameter.

In the large-spreading regime, $\chi_{\rm rel}$ assumes a Lorentzian shape. The broadening of the wavepacket as a function of t is summarized as follows:

$$\Delta r_{\rm rel}(t)=\begin{cases}\Delta r^{(0)}_{\rm rel}=\dfrac{v_{\rm rel}}{\Gamma}\,, & t\ll t^{(\rm spr)}_{\rm rel}\,,\\[2ex] v^{(\rm spr)}_{\rm rel}t=\dfrac{\hbar t}{\mu\Delta r^{(0)}_{\rm rel}}=\dfrac{\hbar\Gamma}{\mu v_{\rm rel}}t\,, & t\gg t^{(\rm spr)}_{\rm rel}\end{cases} \tag{37}$$

The large-spreading result means that $\Delta p_{\rm rel}=\frac{\hbar\Gamma}{v}=\Delta E_{\rm rel}\frac{dp}{dE}$. Since the initial width of the wavepacket is $\frac{v}{\Gamma}=\hbar/\Delta p_{\rm rel}$, the asymptotic wavefunction is found to be at its minimum uncertainty state (MUS) approximately at $t=0$.

The pulse parameters must be taken with a view to minimizing $\Delta E_{\rm rel}$, the energy variance of the relative-motion wavefunction, so as to minimize $\Delta p_{\rm rel}=\Delta E_{\rm rel}\sqrt{\mu/2E_{\rm rel}}$, where $\mu=m/2$ is the reduced mass of the two atoms: $\Delta E_{\rm rel}$ scales with Γ,Ω_1 and the inverse of the time scale. However, $\Delta E_{\rm rel}$ has a lower bound, since the smaller it is, the longer the time the particle stays in the excited state, and thus the larger the probability of radiative decay (spontaneous emission). Using Raman dissociation with highly monochromatic laser beams, one obtains an $|EPR_+\rangle$-like state, characterized by $s=\Delta x_{\rm rel}/\Delta x_{\rm cm}\gg1$, along with small radiative decay (see App. C).

5. Post-Dissociative Dynamics

5.1. *Radial/angular factorization*

The asymptotic $|\chi_{\rm rel}\rangle$ can be numerically shown to have small $\Delta p_{\rm rel}$ and $\Delta E_{\rm rel}$ in Raman dissociation (see Fig. 10 in App. C). Its form may be approximated as (App. B)

$$\langle \mathbf{r}_{\rm rel}|\chi_{\rm rel}(t)\rangle \approx \int dE b(E) e^{-iEt/\hbar} \frac{e^{ikr_{\rm rel}}}{2ikr_{\rm rel}} \times \sum_{l,m} e^{i(\frac{\pi l}{2}+\delta_l(\langle E\rangle))} Y_{l,m}(\theta,\phi)\,. \tag{38}$$

This approximation is justified at low initial l, the spectral amplitudes $b_{l,m}(E)$ (and hence the mean relative energy $\langle E_{\rm rel}\rangle$) and phase-shifts have little dependence on angular momentum. Due to this radial/angular *factorization*,

$$\Delta x_{\rm rel} = \sqrt{\langle x_{\rm rel}^2\rangle - \langle x_{\rm rel}\rangle^2} = \sqrt{\langle r_{\rm rel}^2\rangle\langle\cos^2\,\theta\rangle - \langle r_{\rm rel}\rangle^2\langle\cos\,\theta\rangle^2} > \langle r_{\rm rel}\rangle\Delta(\cos\,\theta) \tag{39}$$

where θ is the angle between $\mathbf{r}$ and the x axis. Thus, for a spherically uniform distribution, $\Delta x_{\rm rel} \approx \langle x_{\rm rel}\rangle$, and similarly, $\Delta(p_x)_{\rm rel} \approx \langle (p_x)_{\rm rel}\rangle$. Since $r_{\rm rel} \approx p_{\rm rel}t/m$ and $\Delta r_{\rm rel} \approx \Delta p_{\rm rel}t/m$, one has

$$\Delta x_{\rm rel}/\Delta r_{\rm rel} \approx \Delta p_{x_{\rm rel}}/\Delta p_{\rm rel} \gg 1\,. \tag{40}$$

Thus, the uncertainty product $s = \hbar\Delta r_{\rm cm}/\Delta p_{\rm rel}$ is replaced by the much smaller $s = \Delta x_{\rm cm}/(\Delta p_x)_{\rm rel}$. To remedy this problem we need a very narrow angular distribution of the receding fragments.

5.2. *Producing 1D correlations by post-selection*

As the angular distribution becomes more sharply peaked around $\theta = 0$, $\Delta x_{\rm rel} \to \Delta r_{\rm rel}$, we are nearing the optimal situation, where $\Delta x_{\rm rel} \approx \Delta r_{\rm rel}$, $\Delta(p_{\rm rel})_x \approx \Delta p_{\rm rel}$. This is achievable by confining the atoms to a cylindrical waveguide[20] of length $2L$ and radius $R = L\tan\alpha$, lying along the x direction (Fig. 4). The slits will only negligibly affect $\Phi_{\rm cm}$ and its entanglement with $\chi_{\rm rel}$ on the x axis, as $\Delta p_{x_{\rm cm}} \ll \langle p_{\rm rel}\rangle$, provided $\alpha \ll 1$. On the other hand, they will affect the shape of $\chi_{\rm rel}$. If the "cylinder" is long enough, $\langle k_{\rm rel}\rangle L \gg 1$, the effect on $\langle \mathbf{r}_{\rm rel}|\psi_{\rm rel}\rangle$ and $\langle \mathbf{p}_{\rm rel}|\psi_{\rm rel}\rangle$ can be approximated by truncating the angular distribution at $\theta = \alpha$, hence

$$(\Delta p_x)_{\rm rel} \approx \left(\frac{p_{x_{\max}} - p_{x_{\min}}}{2}\right)_{\rm rel} = \frac{\langle p_{\rm rel}\rangle(1-\cos\,\alpha) + \Delta p_{\rm rel}(1+\cos\,\alpha)}{2}\,. \tag{41}$$

At small α,

$$\alpha^2 = 4\,\frac{\Delta p_{\rm rel}}{\langle p_{\rm rel}\rangle} = \frac{2\Delta E_{\rm rel}}{E_{\rm rel}} \tag{42}$$

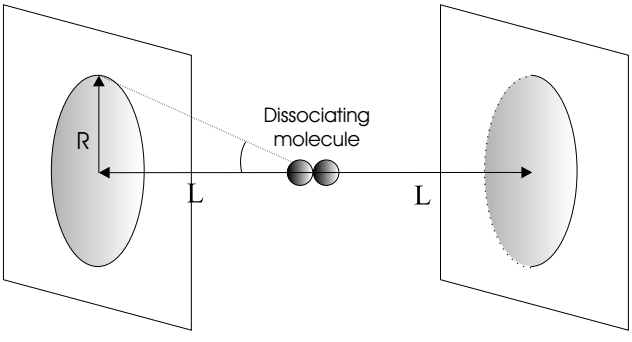

Fig. 4. Geometrical waveguides with slits for quasi-1D dissociation.

is required in order to obtain the optimal ratios $\Delta p_x = 2\Delta p_{\rm rel}$ and $\Delta x = 2\Delta r_{\rm rel}$.

Atom pairs which have passed through the slits are correlated along the x direction, and our 1D analysis may now be applied to their dynamics.

5.3. *Free expansion*

The center of mass distribution of the molecule prior to dissociation is characterized by transverse temperature $T_{\rm cm}$. The post-dissociative momentum distribution $\tilde{\phi}_{\rm cm}(p_{\rm cm})$ is therefore a Gaussian, $\exp[-p_x^2/2\Delta p_x^2]$, where $\Delta p_x \simeq \sqrt{2Mk_BT_{\rm cm}}$.

For $\tilde{\chi}_{\rm rel}(p_{\rm rel})$ we take the asymptotic form (C9), hence the wavefunction at large t is obtained by evolving it in $V = 0$. In Raman dissociation, $\tilde{\chi}_{\rm rel}(p_{\rm rel})$ has a deformed Gaussian distribution, for which the defined measures of entanglement are still appropriate.

5.4. *Storing the 2-particle wavefunction by receding harmonic wells*

Due to the dispersion discussed above, the position and momentum correlations weaken after dissociation, and one must try to restore the initial degree of entanglement by focusing of the 2-particle wavefunction.

When the particles are well-separated and localized near $x = \pm x_0/2$, in a double-trap, with double-parabolic potential

$$V(x) = \frac{1}{2}\, m\omega^2 \left(|x| - \frac{x_0}{2}\right)^2 , \tag{43}$$

the two-particle Hamiltonian has a term

$$\begin{aligned} V_{12}(x_1, x_2) &= \frac{1}{2} m\omega^2 \left(|x_1| - \frac{x_0}{2}\right)^2 + \left(|x_2| - \frac{x_0}{2}\right)^2 \\ &= \frac{1}{2} M\omega^2 x_{c.m.}^2 + \frac{1}{2}\mu\omega^2 (x_{\rm rel} - x_0)^2 \end{aligned} \tag{44}$$

where $M = 2m$ is the total mass and $\mu = m/2$ is the reduced mass. An initially separated wavefunction of the form (2) will retain its shape while subjected to this potential.

When using a potential as in Eq. (43), we move the potentials, so that $x_0 = v_{\rm rel}t$, where $v_{\rm rel} = \langle p_{\rm rel}\rangle/\mu$. This keeps the particles near the centre of the wells and avoids changing their average velocity. Both $|\Phi_{\rm cm}\rangle$ and $|\chi_{\rm rel}\rangle$ behave as a single particle state in a parabolic potential, and may be individually focused.

The analysis shows that the lost degree of "squeezing" cannot be increased, but it can be preserved, by keeping the particles in the moving parabolic potentials, where Δx and Δp_x oscillate periodically. These must be turned on and start receding (moving apart) *immediately* after dissociation, and left on until measurement of the particles.

The shallowness of optically-induced potentials (typically $\approx 1mK$) drastically limits the momentum uncertainty of particles that can be stored, requiring

$$\Delta p_{\rm rel} \ll \sqrt{2mV_{\rm opt}} \tag{45}$$

where $V_{\rm opt}$ is the depth of the potential.

6. Measuring the EPR Correlations: "Ghost" Diffraction

6.1. *Verifying coordinate correlations*

Storage in a parabolic potential can also be used for measuring both momentum and position correlations. Leaving a particle in a parabolic potential for a quarter of the harmonic period has the effect of "Fourier transforming" the wavefunction, as

$$\langle x|\chi_{\rm rel}(t=\tau/4)\rangle = \sqrt{\frac{m\omega}{\hbar}}\langle p = m\omega x|\chi_{\rm rel}(t=0)\rangle \tag{46}$$

After this quarter period, the new momentum distribution reflects the original x-distribution:

$$\chi_{\rm rel}(x_{\rm rel} - \langle x_{\rm rel}\rangle)\phi_{\rm cm}(x_{\rm cm}) \leftrightarrow \tilde{\chi}_{\rm rel}(p_{\rm rel} - \langle p_{\rm rel}\rangle)\tilde{\phi}_{\rm cm}(p_{\rm cm}) \tag{47}$$

and may be measured by time-of-flight measurement.

6.2. *Time of flight measurements*

Verifying and measuring the EPR correlations may be done by position and momentum measurements of the two particles in large *ensembles* of such pairs. In half the pairs, the two momenta are measured by time-of-flight measurement. In the other half, the positions are measured, using Eq. (47) and time-of-flight measurement. One expects to find $\Delta x_{\mp} = \Delta(x_1 \mp x_2)$ and $\Delta p_{\pm} = \Delta(p_1 \pm p_2)$ to satisfy:

$$\Delta x_{\mp}\Delta p_{\pm} \ll \hbar/2 \tag{48}$$

in the approximate $\mathrm{EPR}_{\mp}$ state, respectively.

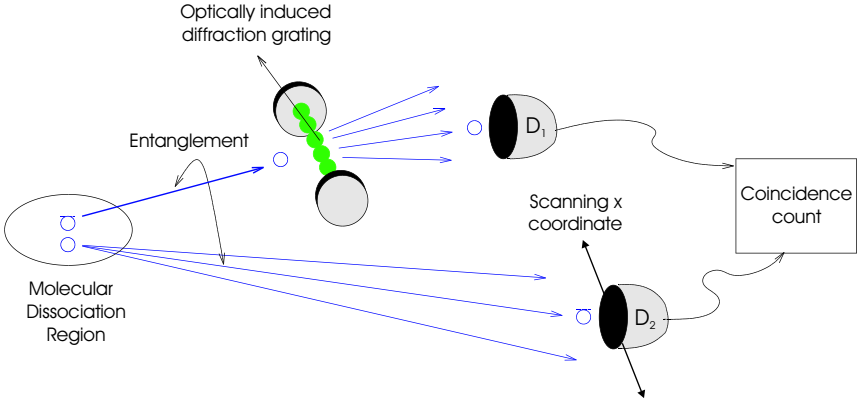

Fig. 5. "Ghost" diffraction setup.

6.3. *Ghost diffraction measurements*

A more elegant measurement scheme uses what has been termed "ghost" diffraction.[17] In this scheme (Fig. 5), the two particles are spatially separated and EPR-correlated (in either the "EPR$_-$" or "EPR$_+$" state) along the x dimension, $\hat{p}_{1x} \pm \hat{p}_{2x} = 0$. Both particles possess the same momentum component in the positive z direction, $p_{1z} = p_{2z} \equiv p_z \gg \Delta p_x$. Particle 1 is diffracted through a (light-induced) diffraction "grating" perpendicular to the z axis, while the path of particle 2 is unobstructed. Detectors D_1 and D_2 are placed far away from the source so as to detect the respective particles. If D_1 is fixed at x_1 and D_2 is moved along the x axis through repeated trials over an *ensemble* of EPR pairs, the two-detector coincidence rate gives a typical diffraction pattern as a function of the D_2 location,

$$\mathcal{P}(x_2|x_1) = \mathcal{P}_0 \left(\frac{\sin\,\beta}{\beta}\right)^2 \left(\frac{\sin\,N\gamma}{N\,\sin\,\gamma}\right)^2 . \tag{49}$$

Here $\mathcal{P}(x_2|x_1)$ is the conditional probability for a hit at D_2 given that D_1 is hit, $\mathcal{P}_0$ a constant, $\gamma = pd(x_1 + x_2)/2\hbar L_2$, N is the number of "slits", w is the slit width and d is the lattice spacing, $\beta = pw(x_1 + x_2)/2\hbar L_2$, L_2 being the sum of the initial distance between particle 2 and the plane of the detector, *and that of particle 1 from the plane of the diffraction grating*. The diffraction pattern occurs even though particle 2 is *unobstructed*.

This two-particle phenomenon may be understood from Fig. 6, which shows its complete analogy with *single*-particle Fraunhoffer diffraction. The reason for the "ghost" interference lies in the symmetry of the source and target in Fraunhoffer diffraction.

A perfect correlation between the particles' momenta would lead to a sharp interference pattern. However, for states with a finite but large s parameter, an uncertainty $\Delta\theta = \Delta p_{2x}^{(c)}/p_z$ is introduced into the trajectory in Fig. 6, $\Delta p_{2x}^{(c)}$ being the *conditional* uncertainty (which is here the smaller of $\Delta p_{\rm rel}$ and $2\Delta p_{\rm cm}$). The

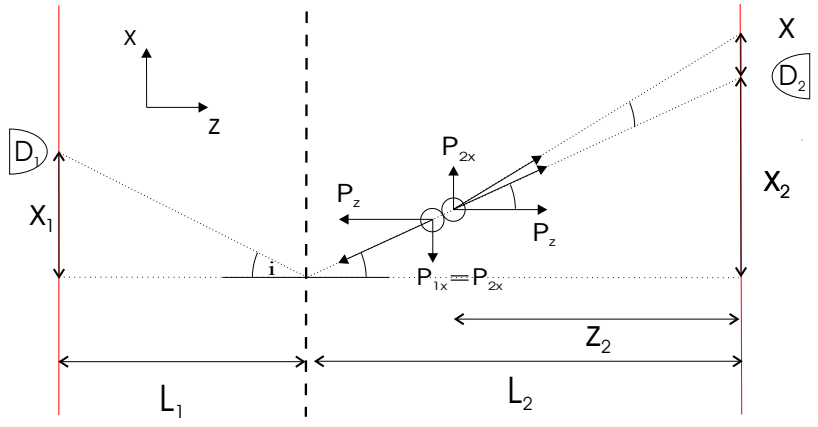

Fig. 6. Fraunhoffer analogy to ghost diffraction.

diffraction pattern is smeared (in particular, the central peak is broadened) by a width

$$\Delta x = z_2 \frac{\Delta p_{2x}^{(c)}}{p_z} \tag{50}$$

from which one obtains the size of $\Delta p_{2x}^{(c)}$.

7. Teleportation

7.1. *Measurement of two-particle continuous variables*

Obtaining a pair of correlated EPR particles (particles 2 and 3 in Fig. 7), as discussed above, is the first stage in the protocol of quantum teleportation of continuous variables.[18,19] The second stage is the measurement of the quantities $\hat{x}_- \equiv \hat{x}_1 - \hat{x}_2$ and $\hat{p}_+ \equiv \hat{p}_1 + \hat{p}_2$ (the "Bell operators").

Opatrný and Kurizki[7] suggested performing the essentially non-local measurement of the Bell operators by a collision between the particles, followed by local measurements of the momenta. Figure 8 schematically shows the scattering of the 'relative' coordinate, assuming a hard-sphere interaction potential, in the classical limit ($\lambda_{dB} \ll R$, where λ_{dB} is the de-Broglie wavelength of the particle and R is the radius of the hard sphere). The impact parameter x_- is related to the angle of deflection by

$$\theta = \pi - 2\,\sin^{-1}(x_-/R)\,. \tag{51}$$

Since θ is the angle of the post-collisional $\mathbf{p}'_-$, and since $\mathbf{p}'_+ = \mathbf{p}_+$, measuring p'_1 and p'_2 is equivalent to measuring p'_+ and p'_-, and hence the pre-collisional p_{x+} and x_-. This completes the Bell measurement. One also requires $p_{z-} \gg p_{x-}$, so that the uncertainty in p_{x-} arising from measuring x_- does not significantly change the impact angle.

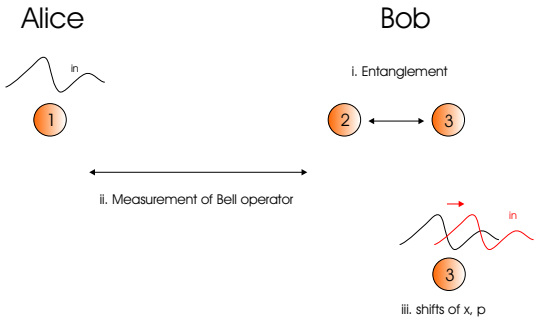

Fig. 7. Scheme of teleportation.

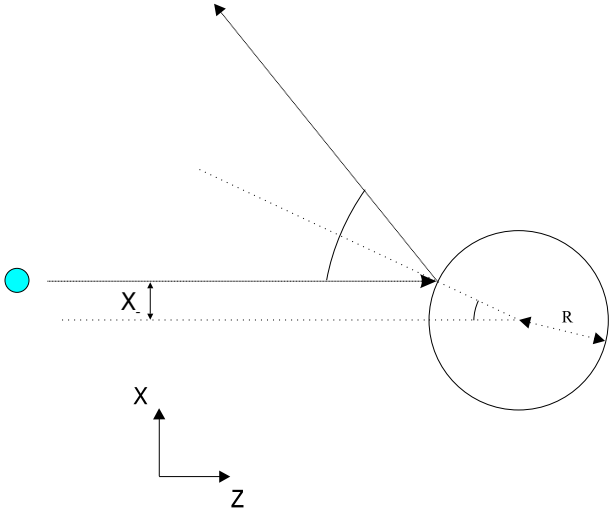

Fig. 8. Hard sphere collision.

7.2. *Fidelity of teleportation*

A measure of the accuracy of teleportation is the fidelity F, the overlap of the input state (the state to be teleported) with the teleported output. The maximal fidelity can be shown to be $F_{\max} = (1 + \Delta x_T \Delta p_T/\hbar)^{-1}$, where Δx_T and Δp_T, are the position and momentum errors incurred during the process. These are

$$\Delta^2 x_T = \Delta^2 x^{(c)} + \Delta^2 x_{\text{meas}} + \Delta^2 x_{\text{shift}}\,, \tag{52}$$

$$\Delta^2 p_T = \Delta^2 p^{(c)} + \Delta^2 p_{\text{meas}} + \Delta^2 p_{\text{shift}}\,, \tag{53}$$

i.e. functions of the error factors in the three stage of teleportation: imperfection of initial entanglement, error in measurement and error in final (momentum and position) shift of the output state. In the molecular association scheme, $\Delta x_{\text{meas}} = \Delta x_{gs}$, and Δp_{meas} is determined by the accuracy of the momentum measurement.

The meaning of the errors Δx_T and Δp_T is that the final Wigner $x-p$ distribution $W_{\rm out}(x_3, p_{x3})$ of the output particle is given by that of the input particle 1, $W_{\rm in}(x_1, p_{x1})$, convoluted with a smoothing function whose width is determined by Δx_T and Δp_T (Refs. 7 and 19):

$$W_{\rm out}(\alpha_3) = \int d^2\alpha W_{\rm in}(\alpha) G_\sigma(\alpha_3 - \alpha)$$
$$\equiv [W_{\rm in} \circ G_\sigma](\alpha_3) \tag{54}$$

where W is presented as a function of a complex variable $\alpha \equiv x + ip$, $\circ$ denotes a convolution and $G_\sigma(\alpha)$ is a complex Gaussian of variance $\sigma = e^{-2s_T}$, $s_T \equiv \hbar/(2\Delta x_T \Delta p_T)$.

8. Conclusions

We have proposed and studied the formation of continuous-variable entanglement in controlled collisions between quasi-free particles, or quantized collective excitations, interacting as fictitious particles, e.g., impurity-atom collisions with Bose-Einstein condenstates (BECs),[14,20,21] or collisions of slow-light polaritons in gases or solids.[13] Cold atoms[10,11] or slow-light polaritons,[13] free to move in 1D, but confined in the remaining 2D by an optical lattice or a waveguide, as well as small-angle collisions of fast-particles,[15] are suitable candidates.

Our comprehensive investigation of collisions has revealed the following striking conclusion: EPR entanglement is *maximized near a scattering resonance*, and grows with the phase-space volume of the initial (uncorrelated) two-system state, up to a limit determined by the spectral distance between resonances.

Specifically, the maximal amount of post-collision entanglement (VN entropy) has been shown to scale logarithmically with the position-momentum uncertainty product (phase-space volume) of the colliding wavepackets, only for *large* wavepacket widths compared to the resonances' width, but less than the distance between resonances. These results[8] show that 1D collisions yield *momentum* entangled states which, in general, *do not resemble* gaussians, but rather interfering multigaussian distributions. Nevertheless, they reveal the quantum information change via collisions of unbound particles. They also specify conditions for the *suppression of decoherence by minimization of the collision-induced entanglement.* Cold-molecule Raman dissociation has been identified as a promising source of EPR gaussian-like entangled states.

Realizations involving *molecular Raman dissociation* have been argued to require the trapping of the fragments, measuring momentum-coordinate correlations (e.g. by diffraction); and finally teleportation by molecular collisions.

Acknowledgments

The support of the European Commission (the QUACS RTN and SCALA NOE) and Israel Science Foundation is acknowledged.

Appendix A. Derivation of the 1D Post-Collision Density Operator

We begin by noting some useful identities for transforming CM coordinate expressions to laboratory-frame expressions:

$$\int dk_1 dk_2 f(k_1,k_2)|k_1,k_2\rangle_{12} = \int dK_{\rm cm} dk_{\rm rel} f(k_1(K_{\rm cm},k_{\rm rel}),k_2(K_{\rm cm},k_{\rm rel}))|K_{\rm cm},k_{\rm rel}\rangle_{\rm cm} \tag{A1}$$

$$\int dK_{\rm cm} dk_{\rm rel} f(k_{\rm rel},K_{\rm cm})|K_{\rm cm},k_{\rm rel}\rangle_{\rm cm} = \int dk_1 dk_2 f(K_{\rm cm}(k_1,k_2),k_{\rm rel}(k_1,k_2))|k_1,k_2\rangle_{12} \tag{A2}$$

where

$$K_{\rm cm} = k_1 + k_2 \tag{A3}$$

$$k_{\rm rel} = \frac{m_2 k_1 - m_1 k_2}{m_1 + m_2} \tag{A4}$$

$$k_1 = \frac{m_1}{m_1+m_2} K_{\rm cm} + k_{\rm rel} \tag{A5}$$

$$k_2 = \frac{m_2}{m_1+m_2} K_{\rm cm} - k_{\rm rel}\,. \tag{A6}$$

We will henceforth treat only particles of equal mass, $m_1 = m_2 \equiv m$. Using Eq. 14, we can insert the appropriate identity element

$$I = \int dK_{\rm CM} dk_{\rm rel} |K_{\rm CM},k_{\rm rel}\rangle\langle K_{\rm CM},k_{\rm rel}| \tag{A7}$$

and integrate over $K_{\rm cm}, k_{\rm rel}$ to obtain:

$$(I_{\rm CM}\otimes \mathsf{S}_{\rm rel})|k_1,k_2\rangle = T\left(\frac{k_1-k_2}{2}\right)\left|k_1+k_2,\frac{k_1-k_2}{2}\right\rangle_{\rm cm} + R\left(\frac{k_1-k_2}{2}\right)\left|k_1+k_2,-\frac{k_1-k_2}{2}\right\rangle_{\rm cm}. \tag{A8}$$

Hence

$$\langle k_1',k_2'|(I_{\rm CM}\otimes \mathsf{S}_{\rm rel})|k_1,k_2\rangle = T\left(\frac{k_1-k_2}{2}\right)\delta[k_1-k_1']\delta[k_2-k_2'] + R\left(\frac{k_1-k_2}{2}\right)\delta[k_1'-k_2]\delta[k_2'-k_1]\,, \tag{A9}$$

so that, for any initial 2-particle state $|\psi_{12}\rangle$,

$$\langle k_1, k_2|(I_{\rm CM} \otimes \mathsf{S}_{\rm rel})|\psi_{AB}\rangle = \int dk_1 dk_2 T\left(\frac{k_1 - k_2}{2}\right)\psi_1(k_1)\psi_2(k_2) + R\left(\frac{k_1 - k_2}{2}\right)\psi_1(k_2)\psi_2(k_1) \tag{A10}$$

Using (A10) we can expand the post-collision two-particle density operator $\tilde{\rho}_{12}$ in the momentum basis:

$$\tilde{\rho}_{12} = \int dk_1 dk_2 dk_1' dk_2' |k_1, k_2\rangle\langle k_1, k_2|(I_{\rm CM} \otimes \mathsf{S}_{\rm rel})|\psi_{12}\rangle \times \langle\psi_{12}|(I_{\rm CM} \otimes \mathsf{S}_{\rm rel})^\dagger |k_1', k_2'\rangle\langle k_1', k_2'| \tag{A11}$$

Taking the trace over particle 2 (which amounts to taking $k_2 \to k_2' \to k$) to obtain the reduced post-collision density operator of particle 1, we have

$$\tilde{\rho}_1 = \int dk_1 dk_1' dk \left(T\left(\frac{k_1 - k}{2}\right)\psi_1(k_1)\psi_2(k) + R\left(\frac{k_1 - k}{2}\right)\psi_1(k)\psi_2(k_1)\right) \times \left(T^*\left(\frac{k_1' - k}{2}\right)\psi_1^*(k_1')\psi_2^*(k) + R^*\left(\frac{k_1' - k}{2}\right)\psi_1^*(k)\psi_2^*(k_1')\right). \tag{A12}$$

Appendix B. Two-Particle Wavepackets via Collisions and Half-Collisions

For a broad class of finite-range interacting potentials,[15,16] one can define a scattering operator taking a wavepacket $|\Psi(0)\rangle$ initially in the "incoming" asymptotic region of a scattering potential $V(\mathbf{r})$ to its final form $|\Psi(t)\rangle$ in the "outgoing" asymptotic region, where $V \to 0$:

$$|\Psi(t)\rangle_{t\to\infty} \to e^{-iH_0 t/\hbar}\mathcal{S}|\Psi(0)\rangle\,, \tag{B1}$$

H_0 being the free ($V = 0$) Hamiltonian. We can write $\mathcal{S} = \Omega_-^\dagger \Omega_+$, where $\Omega_\pm$ are the Möller operators,

$$\Omega_\pm \equiv \lim_{t\to\mp\infty} e^{iHt/\hbar}e^{-iH_0 t/\hbar} \tag{B2}$$

$H = H_0 + V$ being the scattering Hamiltonian. Ω_+ takes the incoming asymptotic wavefunction into the scattering potential, and $\Omega_-^\dagger$ takes it out, to the outgoing asymptotic region.

In half-collision (dissociation) we can relate the asymptotic outgoing wavepacket to the initial bound state $|\Psi(0)\rangle$:

$$|\Psi(t)_{\frac{1}{2}\text{-scat}}\rangle_{t\to\infty} \to e^{-iH_0 t/\hbar}\Omega_-^\dagger|\Psi(0)\rangle\,. \tag{B3}$$

By contrast, for full collisions, we need to specify the *incoming* state at $t \to -\infty$ in order to evaluate the outgoing one at $t \to \infty$. Hence in 'full' collisions, the primary interest lies in finding out the eigenstates of the scattering Hamiltonian

H, which determine the time-dependent dynamics. Each such eigenstate, which we denote $|\Psi^{\pm}_{E,n}\rangle$, completely *overlaps*, in the asymptotic region, with a corresponding eigenstate of H_0, which we call $|\Phi_{E,n}\rangle$. This ensures that a wavepacket *fully localized* in the incoming/outgoing asymptotic region at $t \to -\infty$, and into the outgoing region at $t \to +\infty$, can be expanded as

$$\sum_n \int dE\, c^{\pm}_{E,n}(t=0)e^{-iEt/\hbar}|\Psi^{\pm}_{E,n}\rangle = \sum_n \int dE\, b_{E,n}(t=0)e^{-iEt/\hbar}|\Phi_{E,n}\rangle\,, \quad \text{(B4)}$$

where amplitudes $c^{\pm}$ and b represent the states in the respective bases, enumerated by n.

The energy of the state is conserved during scattering. For spherically symmetrical potentials, such as the molecular potential in the dissociation problem, the angular momentum is conserved, hence $\langle\Phi_{Elm}|\mathcal{S}|\Phi_{E'l'm'}\rangle \propto \delta(E-E')\delta_{l,l'}\delta_{m,m'}$, where the quantum numbers E, l and m are energy and angular momentum eigenvalues now. This means that such an eigenstate merely acquires a phase factor $e^{2i\delta_l}$ under the action of $\mathcal{S}$, where δ_l is the "scattering phase-shift".

Explicitly

$$\langle\mathbf{r}|\Phi_{Elm}\rangle = j_l(r)Y_{lm}(\theta,\phi)\,, \quad \text{(B5)}$$

where $j_l(r)$ is the spherical Bessel function, which has the asymptotic form

$$\lim_{r\to\infty} j_l(r) \propto \frac{\sin(kr-\frac{\pi l}{2})}{kr} = \frac{1}{2ikr}(e^{i(kr-\frac{\pi l}{2})} - e^{-i(kr-\frac{\pi l}{2})})\,, \quad \text{(B6)}$$

where $k = \sqrt{2mE}/\hbar$. For a general potential $V(r) \neq 0$, the scattering solution

$$\langle\mathbf{r}|\Psi_{Elm}\rangle = u_{kl}(r)Y_{lm}(\theta,\phi)\,, \quad \text{(B7)}$$

has the asymptotic form

$$\lim_{r\to\infty} u_{kl}(r) \propto \frac{\sin(kr-\frac{\pi l}{2}+\delta_l)}{kr} = \frac{1}{2ikr}(e^{i(kr-\frac{\pi l}{2}+\delta_l)} - e^{-i(kr-\frac{\pi l}{2}+\delta_l)})\,. \quad \text{(B8)}$$

In accordance with the foregoing discussion, we can write

$$|\Psi^{\pm}_{Elm}\rangle = \Omega_{\pm}|\Phi_{Elm}\rangle = e^{\pm i\delta_l(E)}|\Psi_{Elm}\rangle\,, \quad \text{(B9)}$$

$$c^{\pm}_{Elm} = e^{\pm i\delta_l(E)}b_{Elm} \quad \text{(B10)}$$

since the $c^{\pm}_{Elm}$ wavepacket eigenstates overlap with the b_{Elm} wavepacket of H_0 eigenstates, at $t \to \pm\infty$.

Appendix C. Asymptotic Relative-Motion Wavepackets via Two-Photon (Raman) and One-Photon (Direct) Dissociation

Appendix C.1. *Direct (one-photon) dissociation*

Direct (one-photon)[23] dissociation uses a very short ($\approx 10^{-15}$s) laser pulse to force a transition from the initial, bound vibronic state to a dissociative excited electronic

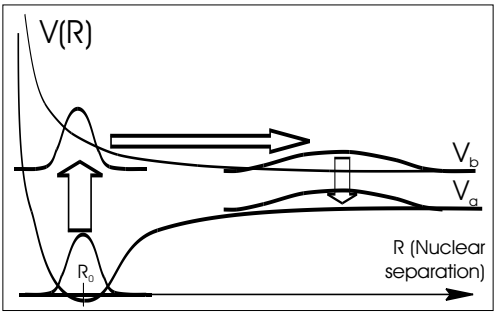

Fig. 9. BO picture of femtosecond photodissociation.

state, i.e. one whose effective potential is repulsive. The physical picture is that the initial wavefunction is "dumped" unchanged onto the excited surface, see (Fig. 9).

Our task is to characterize the change in $|\chi_{\rm rel}\rangle$ as it is scattered to infinity (dissociation). Assuming that the phase-shifts vary little over the energy range of the wavefunction, the important quantity in Eq. (34) is the Franck–Condon factor $\langle\Psi_{Elm}|\chi_{\rm rel}(0)\rangle$. Taking the initial state to be the vibronic ground state, $\langle r_{\rm rel}|\chi_{\rm rel}(0)\rangle$ is a Gaussian. The calculation is carried out semiclassically by approximating the general energy eigenstate $|\Psi_{Elm}\rangle$ with an Airy function in the vicinity of its turning point, and performing the radial overlap integral. For a sufficiently steep dissociative surface and narrow ground-state, one obtains

$$\langle\Psi_{E(lm)}|\chi_{\rm rel}(0)\rangle \simeq \frac{1}{\pi\sqrt{V_e'(x_t)}}\langle x_t(E)|\chi_{\rm rel}(0)\rangle\,, \tag{C1}$$

where $x_t(E)$ is the turning point of the energy eigenstate, and V_e is the potential of the excited electronic state. Eq. (C1) is an approximation known as "Condon reflection", enabling one to estimate $\Delta E_{\rm rel}$ and $\Delta p_{\rm rel}$ of the asymptotic wavefunction:

$$\begin{aligned}\Delta p_{\rm rel} &\cong \Delta x_t \frac{dp}{dx_t}\bigg|_{x_t=x_0} \\ &\cong \Delta x_{g.s.} \frac{dE}{dx_t}\bigg|_{x_t=x_0} \Big/ \frac{dE}{dp}\bigg|_{E=V_g(x_0)} \\ &= \sqrt{\frac{2\hbar}{8(V_g(x_0)-E_{dis})}}\cdot\left(\frac{\mu}{V_a''(x_0)}\right)^{\frac{1}{4}}\cdot V_g'(x_0)\end{aligned} \tag{C2}$$

and the wavefunction will have the approximate form

$$\langle p|\chi_{\rm rel}\rangle \to e^{-(\frac{p-p_0}{2\Delta p})^2} \tag{C3}$$

where $p_0 = \sqrt{2\mu V_e(x_0)}$.

Numerical results were obtained for the femtosecond direct (single-photon) dissociation via transition $X \to D$ in Na_2, using the Numerov method to obtain

the energy eigenstates $|\psi_{Elm}\rangle$. Equation (C1) and the full calculation give roughly the same result, $\Delta E_{\rm rel} = 2.12{\times}10^{-3}$ E_h, $\Delta p_{\rm rel} = 3.497$ a.u., corresponding to a minimum uncertainty spread (MUS) with $\Delta x_{\rm rel} = 0.286$ bohr.

The values for $\Delta E_{\rm rel}$, $\Delta p_{\rm rel}$ are too large for storing the wavepacket in a light-induced potential, for which only Raman dissociation is appropriate, as shown below.

Appendix C.2. *Raman (Two-Photon) Dissociation*

The stimulated Raman Hamiltonian is written as

$$H_{\rm tot} = H_{\rm mol} - 2\mu_1 \cdot \hat{\epsilon}_1 \epsilon_1(t)\cos(\omega_1 t) - 2\mu_2 \cdot \hat{\epsilon}_2 \epsilon_2(t)\cos(\omega_2 t)\,. \tag{C4}$$

Here $H_{\rm mol}$ is the molecular Hamiltonian, $\epsilon_1(t)$ and $\epsilon_2(t)$ are slowly varying electric field amplitudes, μ_1 and μ_2 are the electronic transition dipoles.

We need to calculate b_1 and b_2, the amplitudes of the bound vibronic states 1 and 2, in the interaction representation, and b_{Elm}, those of the continuum levels states $|\Psi_{Elm}\rangle$, as a function of the two-photon (Raman) Δ_1 detuning from the level 1-2 transition. Making the spectrally 'flat continuum' approximation, one finds that the time-dependence of $b \equiv (e^{i\Delta_1 t}b_1, b_2)$ is governed by an effective Hamiltonian

$$H = \hbar \begin{pmatrix} -\Delta_1 & \Omega_1(t) \\ \Omega_1(t) & -i\Gamma(t) \end{pmatrix}, \tag{C5}$$

where

$$\Gamma(t) = \pi \sum_{l,m} |\langle E - \hbar\omega_2 | \mu_2 | 2\rangle|^2 \epsilon_2(t)^2/\hbar \tag{C6}$$

$$\Omega_1(t) = \langle 1|\mu_1|2\rangle \epsilon_1(t)/\hbar\,. \tag{C7}$$

The $-i\Gamma$ term represents the coupling to the continuum and causes exponential decay in the population of the bound states. The coefficients $b_{Elm}(t)$ which we seek are obtained from $b_2(t)$ via

$$b_{E,m}(t) = -i \int_0^t dt' \Omega^*_{2,E,m}(t') e^{i\Delta_E t'} b_2(t')\,. \tag{C8}$$

For rectangular pulse envelopes of the fields near ω_1 and ω_2, the dynamics of the system is that of a 2-level Rabi oscillation, combined with exponential decay. Γ and Ω_1 are time-independent and one readily obtains

$$b_{Elm}(t \to \infty) = -i \frac{\Omega_1 \Omega^*_{2_{E-\hbar\omega_2,l,m}}}{(\Delta_E + \Delta_1/2 + i\Gamma/2)^2 - \Omega^2_{\rm eff}/4} \tag{C9}$$

where $\Omega_{2_{Elm}} = \langle 2|\mu_2|Elm\rangle \epsilon_2/\hbar$.

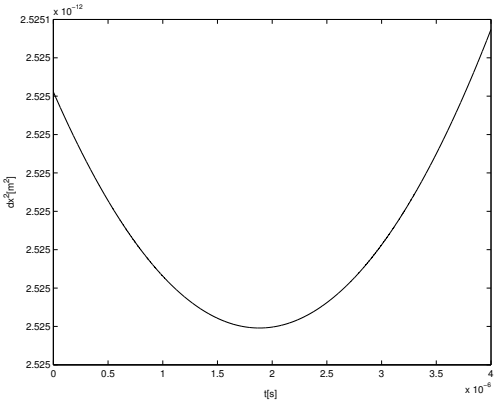

Fig. 10. Broadening of Raman-dissociated internuclear wavefunction as a function of time for the given parameters.

This qualitative analysis does not take into account factors such as spontaneous emission and time-dependence of the pulse envelope. One may calculate the resulting wavefunction using the adiabatic approximation,

$$\begin{pmatrix} b_1(t) \\ b_2(t) \end{pmatrix} \begin{pmatrix} e^{-i\Delta_1 t} \cos\theta(t) \\ \sin\theta(t) \end{pmatrix} e^{i\int_0^t \mathcal{E}_1(t')dt'} \tag{C10}$$

where

$$\theta(t) = \frac{1}{2} \arctan\left(\frac{2\Omega_1}{i\Gamma - \Delta_1}\right) \tag{C11}$$

where Δ_1 is the detuning of ω_1, and

$$\mathcal{E}_{1,2} = \frac{1}{2}\{\Delta_1 + i\Gamma_2 \pm [(\Delta_1 - i\Gamma_2)^2 + 4\Omega_1^2]^{\frac{1}{2}}\}\,. \tag{C12}$$

The conditions for high accuracy of the adiabatic approximation hold for the Gaussian pulses Gaussian pulses $\epsilon_{1,2}$ such that

$$\Omega_1(t) = \Omega_1^0 e^{-\frac{1}{2}(\frac{t-t_1}{\Delta\tau})^2} \tag{C13}$$

$$\Gamma(t) = \Gamma^0 e^{-\frac{1}{2}(\frac{t-t_2}{\Delta\tau})^2}\,. \tag{C14}$$

Typical parameters are $\Delta_1 = 0$, where $\Delta\tau = 0.4\mu$s, $t_1 = 0.2\mu$s, $t_2 = 2.5\mu$s, and the maximal intensities are $I_1 = 5\mathrm{W/cm}^2$ and $I_2 = 5 \times 10^4\mathrm{W/cm}^2$. These give the values $\Omega_1^0 = 1.77169 \times 10^{10}\mathrm{s}^{-1}$ and $\Gamma^0 = 2.5 \times 10^{10}\mathrm{s}^{-1}$, calculated for the discrete levels $v = 28, e = X$ (electronic ground state) and $v = 37, e = A$ (excited state), where beam 2 is tuned to resonance with the continuum energy corresponding to $T = 5K$. The "counterintuitive" pulse sequence is advantageous in that it allows level 2 to be populated for a very short time period, minimizing the probability for its spontaneous decay to state 1.

For the above parameters, $\Delta E_{\rm rel} = \hbar \cdot 3.2645 \times 10^8 {\rm s}^{-1}$, and the particle spends a total time $\int dt |b_2(t)|^2 = 0.0157\tau$, where $\tau = 12.6$ns is the theoretical lifetime of level 2.[22]

References

1. A. Einstein, B. Podolsky and N. Rosen, *Phys. Rev.* **47**, 777 (1935).
2. E. Schröedinger, *Proc. Cambridge Philos. Soc.* **32**, 446–452 (1936).
3. K. W. Chan and J. H. Eberly, quant-ph/0404093 v2 (2004); C. K. Law and J. H. Eberly, *Phys. Rev. Lett.* **92**, 127903 (2004).
4. J. Eisert, C. Simon and M. B. Plenio, *J. Phys. A* **35**, 3911 (2002); H. Mack and M. Freyberger, *Phys. Rev. A* **66**, 042113 (2002); S. Parker, S. Bose and M. B. Plenio, *ibid.* **61**, 032305 (2000); P. Horodecki and M. Lewenstein, *Phys. Rev. Lett.* **85**, 2657–2660 (2000).
5. S. L. Braunstein, *Phys. Rev. Lett.* **80**, 4084 (1998); S. L. Braunstein and H. J. Kimble, *ibid.* **80**, 869 (1998).
6. J. C. Howell, R. S. Bennink, S. J. Bentley and R. W. Boyd, *Phys. Rev. Lett.* **92**, 210403 (2004).
7. T. Opatrný and G. Kurizki, *Phys. Rev. Lett.* **86**, 3180 (2001).
8. A. Tal and G. Kurizki, *Phys. Rev. Lett.* **94**, 160503 (2005).
9. A. Vardi and M. Shapiro, *J. Chem. Phys.* **104**, 5490 (1996).
10. T. Opatrny, B. Deb and G. Kurizki, *Phys. Rev. Lett.* **90**, 250404 (2003).
11. G. K. Brennen *et al.*, *Phys. Rev. Lett.* **82**, 1060 (1999); D. Jaksch *et al.*, *ibid.* **85**, 2208 (2000); C. Moura Alves and D. Jaksch, *ibid.* **93**, 110501 (2004); I. H. Deutsch *et al.*, *Fortschr. Phys.* **48**, 925–943 (2000).
12. M. Fedorov *et al.*, *Phys. Rev. A* **69**, 052117 (2004).
13. M. Masalas and M. Fleischhauer, *Phys. Rev. A* **69**, 061801 (2004); I. Friedler, G. Kurizki and D. Petrosyan, *Europhys. Lett.* **68**, 625 (2004).
14. I. E. Mazets, G. Kurizki, N. Katz and N. Davidson, *Phys. Rev. Lett.* **94**, 190403 (2005).
15. M. L. Goldberger and K. M. Watson, *Collision Theory* (Dover Publications Inc., New York, 2004).
16. L. D. Landau and E. M. Lifshitz, *Statistical Physics* (Butterworth-Heinemann, Oxford, 1980).
17. D. V. Strekalov, A. V. Sergienko, D. N. Klyshko and Y. H. Shih, *Phys. Rev. Lett.* **74**, 3600 (1995).
18. L. Vaidman, *Phys. Rev. A* **49**, 1473 (1994).
19. S. L. Braunstein and H. J. Kimble, *Phys. Rev. Lett.* **80**, 869 (1998).
20. T. Esslinger *et al.*, *Phys. Rev. Lett.* **94**, 210401 (2005); H. Ito *et al.*, *Phys. Rev. Lett.* **76**, 4500 (1996).
21. W. Ketterle, D. S. Durfee and D. M. Stamper-Kurn, *Proceedings of the International School of Physics "Enrico Fermi"*, Course CXL, eds. M. Inguscio, S. Stringari and C. E. Wieman (IOS Press, Amsterdam, 1999), pp. 53–55.
22. W. J. Stevens *et al.*, *J. Chem. Phys.* **66**, 1477 (1977).
23. B. M. Garraway *et al.*, *Rep. Prog. Phys.* **58**, 365 (1995).